Integrative Biology

Quantitative biosciences from nano to macro

www.rsc.org/ibiology

Volume 1 | Number 5–6 | June 2009 | Pages 337–436

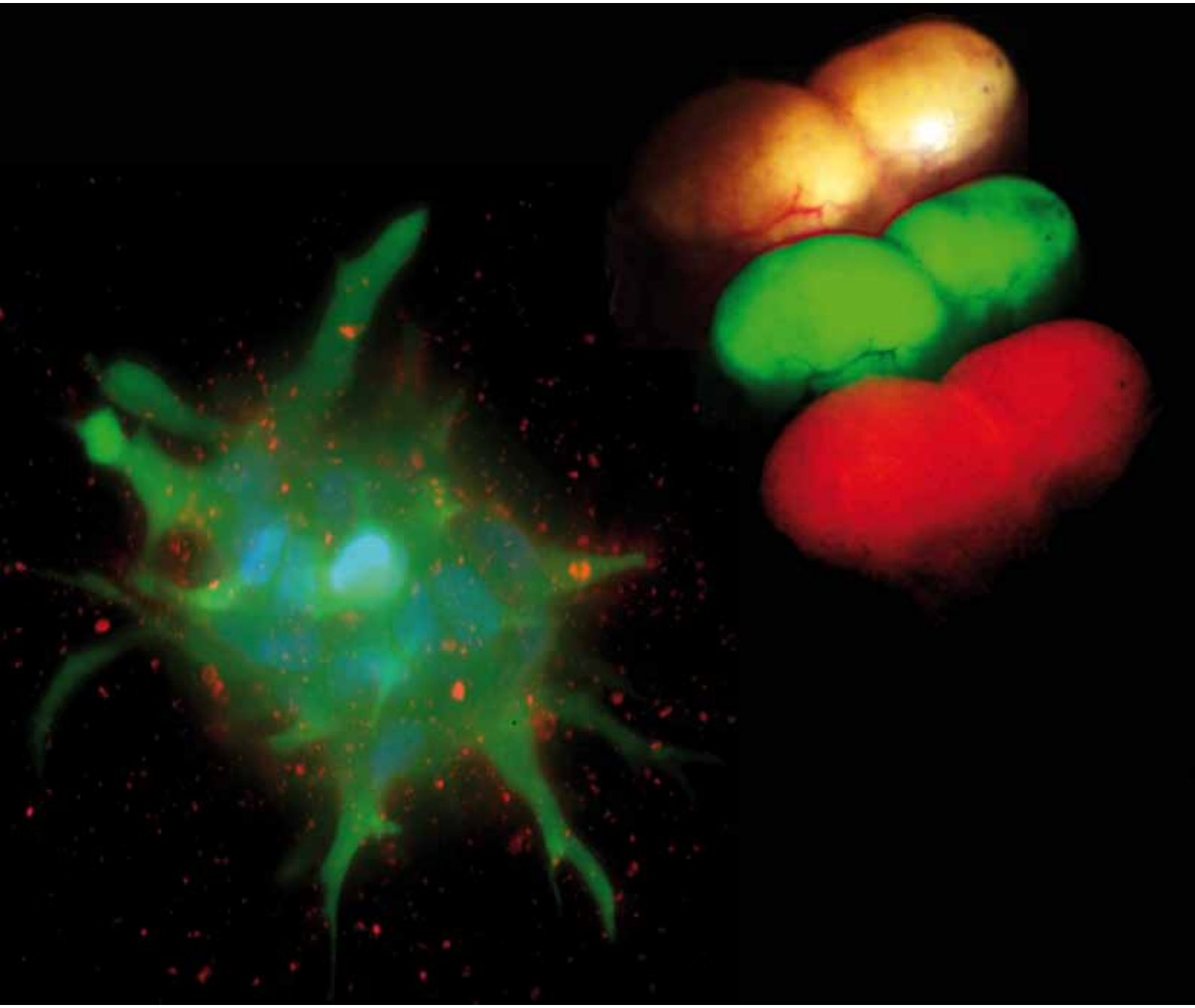

ISSN 1757-9694

RSC Publishing

Aguilera and Tsien
Cell-penetrating peptides in cancer

Stachowiak
Brain neurogenesis and nanomediated gene transfer

1757-9694(200905/06)1:5/6;1-U

Systemic *in vivo* distribution of activatable cell penetrating peptides is superior to that of cell penetrating peptides†

Todd A. Aguilera,‡[ab] Emilia S. Olson,‡[ab] Margaret M. Timmers,[a] Tao Jiang[ac] and Roger Y. Tsien*[ac]

Received 10th March 2009, Accepted 29th April 2009
First published as an Advance Article on the web 11th May 2009
DOI: 10.1039/b904878b

Cell penetrating peptides (CPPs) have been developed as vehicles for payload delivery into cells in culture and in animals. However several biologic features limit their usefulness in living animals. Activatable cell penetrating peptides (ACPPs) are polycationic CPPs whose adsorption and cellular uptake are minimized by a covalently attached polyanionic inhibitory domain. Cleavage of the linker connecting the polyanionic and polycationic domains by specific proteases (tumor associated matrix metalloproteases discussed herein) dissociates the polyanion and enables the cleaved ACPP to enter cells. In contrast to their CPP counterpart, ACPPs are relatively nonadherent and distributed uniformly to normal tissues. While nonaarginine (r_9) CPP administered intravenously into mice initially bind to the local vasculature and redistribute to the liver, where >90% of the injected dose accumulates 30 min after injection. Regardless of the presence of the polyanionic inhibitory domain, confocal imaging of live tissues reveals that the majority of the ACPP and CPP remain in punctate organelles, presumably endosomes. Therefore further improvements in the efficiency of delivery to the cytosol and nucleus are necessary. In addition to improved target specificity, a major advantage of ACPPs over CPPs for potential clinical applications is reduced toxicity. Systemically administered r_9 CPP causes acute toxicity in mice at a dose 4-fold lower than the MMP cleavable ACPP, a complication not observed with an uncleavable ACPP presumably because the polycationic charge remains masked systemically. These data suggest that ACPPs have greater potential than CPPs for systemic delivery of imaging and therapeutic agents.

Introduction

Polycationic cell penetrating peptides (CPPs), also known as protein transduction domains (PTDs), have been proposed for many years as vehicles for intracellular delivery of payloads from small polar molecules to large macromolecules and nanoparticles.[1,2] Most published successes have been on model membranes or cells in culture, though clinically relevant delivery of drugs or contrast agents will require *in vivo* efficacy. Early reports that systemic administration could give efficient intracellular delivery need re-examination because cell uptake was assessed after fixation, which is now known to enable entry into cells.[3–5] In most efficacious *in vivo* applications of CPPs, the peptides were locally injected into tumors[6,7] or into the peritoneum to deliver to intraperitoneal (IP) tumors.[8,9]

In this report we describe *in vivo* pharmacokinetic and toxicity problems of CPPs and show that many of them can be ameliorated by conversion to activatable CPPs (ACPPs). ACPPs consist of a polycationic CPP (typically arg_9 or r_9)

[a] *Department of Pharmacology, University of California at San Diego, La Jolla, CA 92093-0647, USA*
[b] *Medical Scientist Training Program, University of California at San Diego, La Jolla, CA 92093-0606, USA*
[c] *Howard Hughes Medical Institute, and University of California at San Diego, La Jolla, CA 92093-0647, USA. E-mail: rtsien@ucsd.edu*
† Electronic supplementary information (ESI) available: Supplemental Figures 1–3 and LC mass spectra for peptides used in the study. See DOI: 10.1039/b904878b
‡ These authors contributed equally.

Insight, innovation, integration

Polycationic cell penetrating peptides (CPPs) have been touted as vehicles for payload (drugs, imaging agents, *etc.*) delivery into cells in culture and animals because of their electrostatic adsorption to cell surfaces and subsequent endocytosis. We have found that masking a CPP, in this case a positively charged polyarginine with a negatively charged polyglutamate, and making it activatable (ACPP) with an enzyme cleavable linker can overcome pharmacologic disadvantages, such as limited distribution and toxicity. This study provides the foundation for enhancing specific cell uptake of CPPs by selectively unmasking them in diseased tissue where targeted proteases are expressed. ACPPs could be applied to targeted nanotechnology, diagnostic imaging, and therapeutic development.

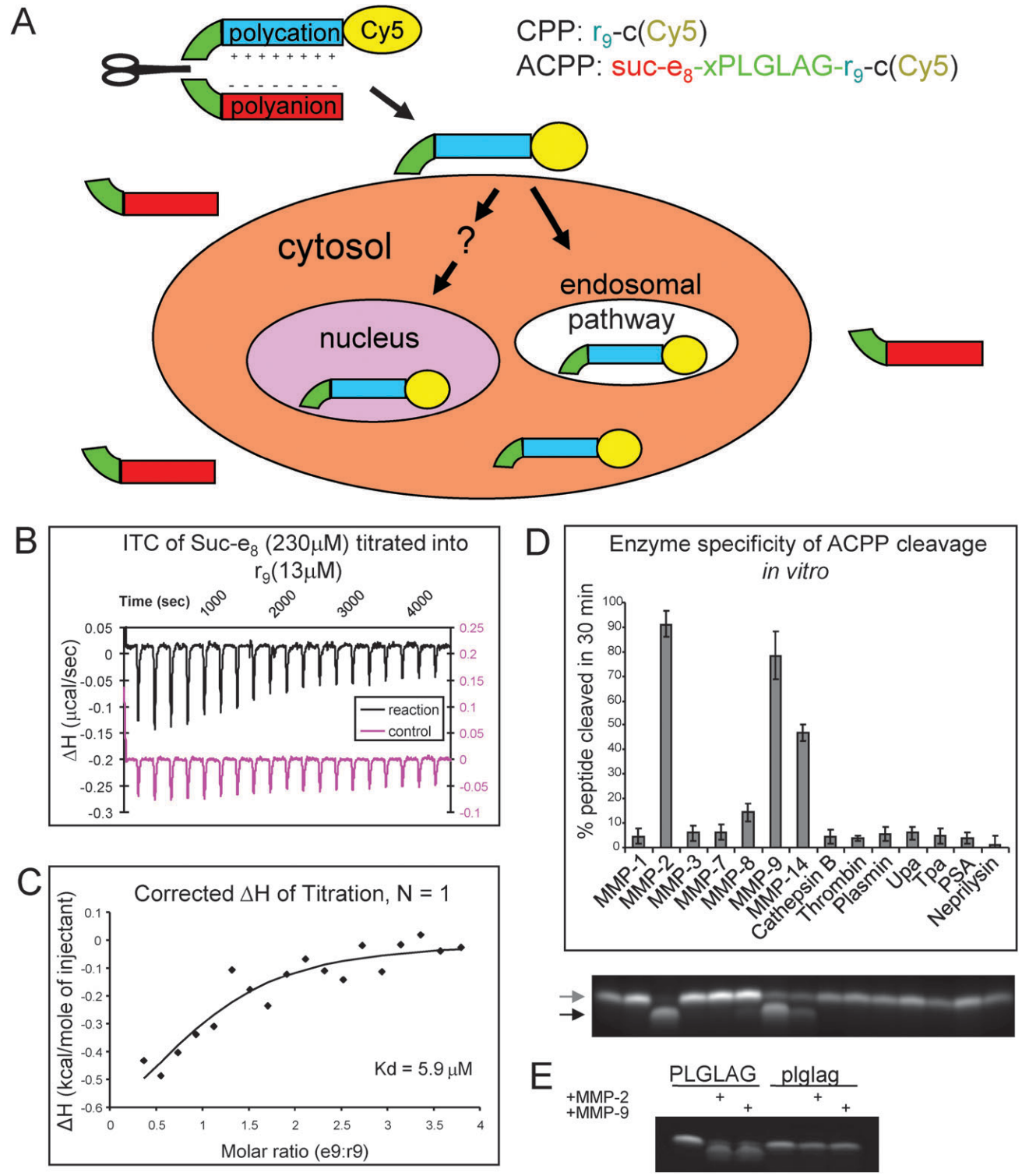

Fig. 1 ACPPs selectively unmask CPPs upon protease cleavage of a linker, which is selective for MMPs when the linker sequence is PLGLAG. (A) General scheme for ACPPs. While the linker (green) between the polyanion (red) and polycation (blue) sequences remains intact, cell uptake is blocked and the entire molecule can enter the extracellular space of tissues and wash out. Once a protease (symbolized by a scissor) cuts the linker, the polyglutamate dissociates, allowing the polyarginine and its payload (yellow, in current examples Cy5) to immediately adhere to cells and eventually become endocytosed. (B) Isothermal titration calorimetry raw data showing the change in enthalpy as 230 μM Suc-e_8 is titrated into a 13 μM solution of r_9. (C) These raw data can be corrected for and the change in enthalpy can be plotted as a function of molar ratio of the two peptides yielding determination of the K_d. (D) The percentage by which the polycation is released as a result of cleaving the PLGLAG linker after 30 min incubation with 50 nM protease. Cleavage of the peptide was detected by tricine SDS-PAGE; a representative fluorescence image of a gel is shown below with the first lane being uncleaved peptide. The following lanes line up with the chart above. Arrows point to uncleaved peptide (upper gray arrow) and cleaved peptide (lower black arrow). Error bars are standard deviation from $n = 3$. (E) D-amino acid control Suc-e_8-*x*plglag-r_9-c(Cy5) remains uncut by MMP-2 and MMP-9 under conditions where the ACPP Suc-e_8-*x*PLGLAG-r_9-c(Cy5) is cleaved.

connected *via* a cleavable linker to a matching polyanion (typically glu_9 or e_9), which reduces the net charge to nearly zero and thereby inhibits adhesion and uptake into cells. Lower case letters indicate D-amino acids, which are preferred within the polyanion and polycation to minimize proteolysis. Upon cleavage of the linker, the polyanion is released, locally unmasking the polyarginine and its inherent adhesiveness (Fig. 1A).[10a] This mechanism implies that the affinity of the polyglutamate for the polyarginine is strong enough for efficient intramolecular hairpin formation, yet weak enough to dissociate after linker cleavage. Before discussing the pharmacokinetics and toxicity in animals, we discuss validation of multiple components of the ACPP design. We now show by isothermal calorimetry that the dissociation constant of e_9 for r_9 is in the appropriate range for effective masking of the CPP to be switched on upon cleavage. We also verify the *in vitro* selectivity of our workhorse matrix metalloprotease (MMP) linker, PLGLAG, for cleavage by a wide range of enzymes. Unlike 2-D cultures, 3-D cultures accumulate enough endogenous extracellular proteases to trigger ACPP cleavage and uptake, yet 3-D cultures are still thin and transparent enough to validate protease triggered ACPP accumulation and determine subcellular localization. The question of *in vivo* selectivity is addressed in the companion paper (Olson *et al.*).[10b]

The simple r_9 CPP initially binds to the vasculature at the site of injection then redistributes mainly to the liver, as previously seen with systemic administration of Tat peptide from HIV.[11,12] ACPPs access tissues more broadly, have longer circulation, are excreted by both renal and hepatobiliary routes, are less toxic, and enable targeting to tumors expressing enzymes that cleave the linker. Another controversial issue regarding CPPs is whether they can efficiently deliver cargoes to the cytoplasm and nucleus, not just endosomes or other punctate organelles. Most reports on verifiably live cells in standard two-dimensional tissue culture demonstrate that significant ($>10\%$) escape from endosomes requires at least several micromolar CPP depending upon the cell type and culture conditions.[13] Because our culture models rarely had cytosolic and nuclear uptake of CPP and ACPPs, we have taken an independent approach to determine subcellular localization in animals after systemic injection. We harvest live tissues and image them immediately with confocal microscopy. Live observation is important because after cell death the peptide redistributes to the nucleus in the same way that fixation and cell death are known to permit redistribution of CPPs. We find that at doses below systemic toxicity levels, almost all of the CPP payloads remain within punctate organelles in all tissues imaged. Therefore, improved mechanisms for endosomal escape will be needed to deliver payloads efficiently to the cytosol and nucleus in living animals.

Results

Determining the affinity of arg_9 for glu_9 *in vitro*

In order for the e_9 domain of an ACPP to block cell uptake of the r_9 CPP that could be restored following proteolysis, the r_9 must be intramolecularly complexed with the e_9 while the linker is intact, which means that the dissociation constant of a bimolecular e_9–r_9 complex, K_d, should be much less than the effective molarity (EM) imposed by the linker. A linker of six amino acid residues plus an 6-aminohexanoyl spacer consists of about 25 single bonds, which corresponds to an EM of 49 mM.[14] To test the aforementioned hypothesis that $K_d \ll$ EM for ACPPs, we compared this literature value for EM to an experimental value for K_d determined by isothermal titration calorimetry (ITC). We synthesized model polyanionic (Suc-e_8, where the succinyl group is glutamate without the N-terminal amine) and polycationic (r_9) peptides, both amidated at their C-termini. We measured their mutual affinity by ITC at physiological ionic strength and temperature. The advantage of ITC is that it requires neither spectroscopic labels nor attachment to a solid support, either of which might perturb the affinity. Multiple ITC runs with Suc-e_8 titrated into r_9 or *vice versa* at different concentrations and corrected for heats of dilution gave a K_d of (6 ± 0.7) μM (mean ± s.d.), well below EM = 49 mM as required for essentially complete formation of an intramolecular hairpin. Fig. 1B and C show a representative uncorrected experiment and the corresponding corrected titration curve fit which yielded a K_d in this case of 5.9 μM.

After protease cleavage of the linker, the free concentrations of the e_9 and r_9 must be below the K_d in order for them to substantially dissociate and allow cell uptake of the r_9. Typical doses of ACPPs for optical imaging are 10 nmol per 25 g mouse or 0.4 μmol kg^{-1}. Even if all the ACPP were fully cleaved but none excreted, the total concentration of e_9 and r_9 would be submicromolar, and the free concentrations would be yet lower due to binding to membranes and macromolecules. Cleavage-dependent dissociation of e_9 from r_9 is robust because the intramolecular EM with an intact linker is orders of magnitude higher than the free concentration of each fragment after cleavage.

Selectivity for MMP-2 and MMP-9 *in vitro*

To assess the enzyme selectivity of our initial MMP-cleavable ACPP, Suc-e_8-*x*PLGLAG-r_9-c(Cy5) (*x* = aminohexanoic linker; Cy5 is a deep-red fluorophore for *in vivo* imaging) was incubated for 30 min with 50 nM each of seven MMPs (1, 2, 3, 7, 8, 9 and 14) and seven other enzymes (neprilysin, cathepsin B, urokinase (uPa), tissue plasminogen activator (tPa), thrombin, prostate specific antigen (PSA), and plasmin). The resulting mixtures were then subjected to polyacrylamide gel electrophoresis, separating cleaved product from uncleaved starting material. MMP-2, -8, -9, and -14 all cleaved a significant amount of the peptide, with MMP-2 and -9 causing near complete cleavage after just 30 min (Fig. 1D). These data demonstrate that the PLGLAG substrate is preferentially cleaved by gelatinases MMP-2 and -9 over the other enzymes tested. Under similar conditions, MMP-2 and -9 did not attack a cleavage resistant control with D-amino acid linker *x*plglag (Fig. 1E).

MMP-based ACPPs are selectively taken up by tumor cell clusters in a 3-D culture model

Even though cell lines such as HT-1080 secrete MMP-2 and -9, those enzymes become notably diluted in the supernatants of

traditional two-dimensional culture, causing slow ACPP cleavage and negligible uptake. Previously, we found that significant cleavage and uptake of ACPPs required precleavage with exogenous protease.[10a] A higher-density culture system in which endogenously secreted proteases accumulate sufficiently to mediate localized cleavage and uptake of peptide would be quite useful. Compared to solid tumors *in vivo*, cultures have greater transparency, enable better subcellular resolution of peptide localization, allow for easy discrimination between live and dead cells, and

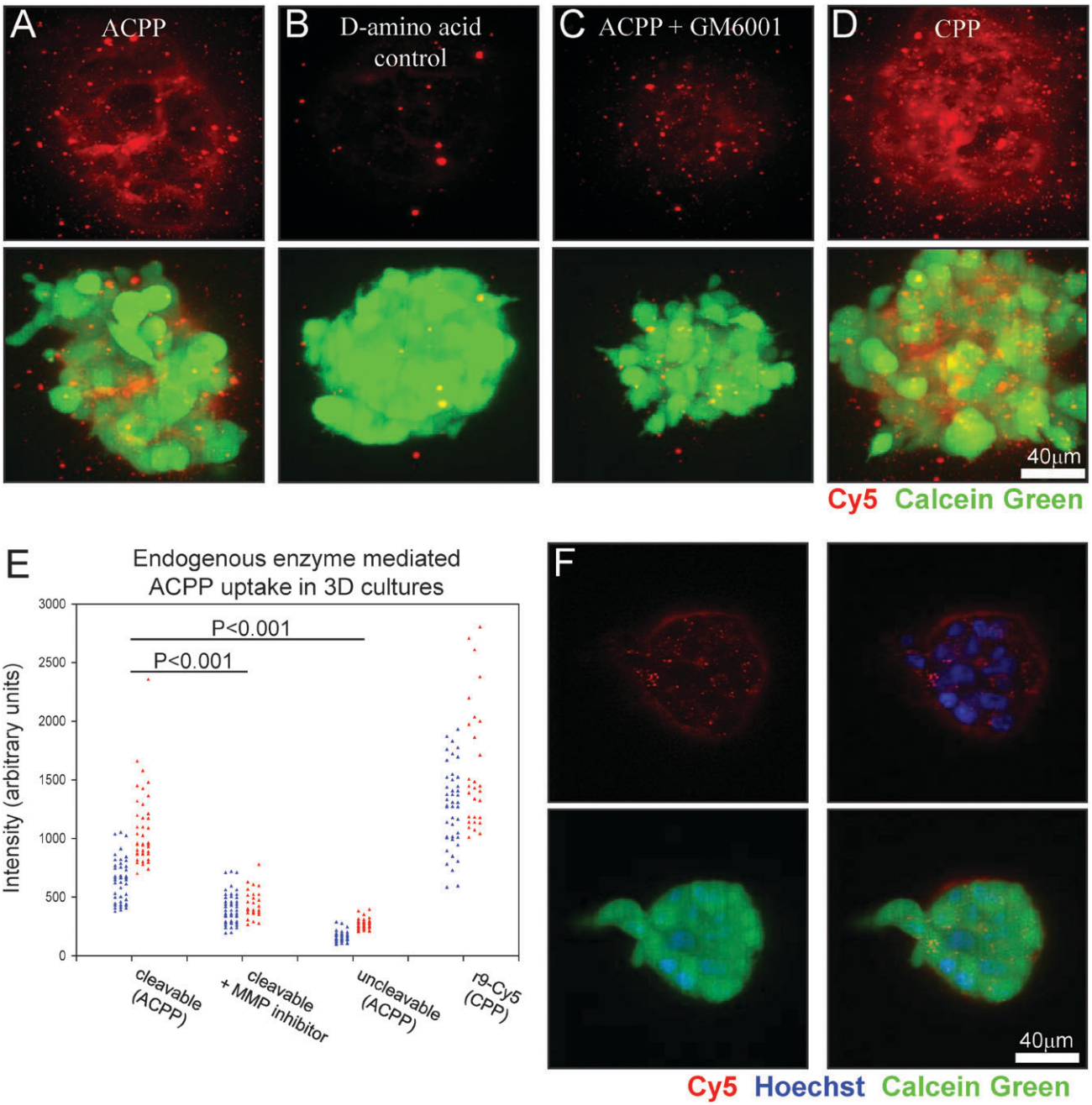

Fig. 2 MMP cleavable PLGLAG linker built into the ACPP shows uptake due to endogenous proteases in a 3-D tissue culture model. (A, B) MDA-MB-231 cluster confocal maximum projections of cleavable PLGLAG ACPP *versus* uncleavable D-amino acid peptide (red) show micro localization of peptide and differential uptake due to the presence of the cleavable linker. (C) Shows decreased cleavable ACPP peptide when co-incubated with 100 μM broad spectrum MMP inhibitor GM6001. (D) r_9Cy5 CPP positive control shows uptake of CPP throughout 3-D clusters. Scale bar for A–D is 40 μm. (E) Comparison of the average intensity of multiple 3-D clusters of HT-1080 fibrosarcoma (red) or MDA-MB-231 mammary adenocarcinoma (blue) cells treated with PLGLAG cleavable ACPP, ACPP + GM6001 MMP inhibitor, uncleavable D-amino acid ACPP, and r_9Cy5 CPP control (t-test p-value for significance labeled accordingly). Cell clusters were incubated with 1.5 μM peptide for 24 h then washed (3×), counterstained with calcein green AM ester (cell viability, green), and then imaged. (F) Representative confocal slice of a 3-D cluster showing ACPP uptake into subcellular puncta, cell surface, and extracellular matrix of live cells. ACPP is shown in red, Hoechst 33342 counter stain for cell nuclei (blue), and calcein green AM (green) to show live cells.

circumvent systemic pharmacokinetics for early validation of imaging peptides. We therefore decided to test a three-dimensional culture model in which invasive cancer cells degrade the extracellular matrix, a process that has been shown to involve MMPs.[15]

We grew MDA-MB-231 human adenocarcinoma cells and HT-1080 human fibrosarcoma cells suspended in matrigel to assay ACPP uptake. Confocal maximum projections in Fig. 2A–D show Cy5 fluorescence (red) from MDA-MB-231 cell clusters treated with cleavable PLGLAG ACPP in the absence and presence of GM6001, a broad-spectrum MMP inhibitor. Also shown are clusters treated with a cleavage-resistant control with a D-amino acid linker (plglag), and a positive control CPP, r_9-c(Cy5), that requires no cleavage. Cells were preloaded with calcein green AM (green fluorescence) to confirm cell viability. The imaging demonstrated that the cleavable ACPP accumulated to levels nearly as high as that of the positive control CPP, and that uptake was significantly diminished upon addition of the MMP inhibitor or replacement of L-amino acids by D-amino acids. 3D culture data was quantified using Cy5 intensities averaged over regions within 20 to 40 3-D clusters of MDA-MB-231 and HT-1080 cells imaged using a fluorescent dissecting microscope (representative experiment shown in Fig. 2E and example of images shown in ESI Fig. S1†). The overall dynamic range between the positive and negative controls was 4- to 10-fold. Upon close examination of the confocal images, cells that proved to be dead based upon counterstain always had nuclear colocalization of peptide whether CPP, ACPP or cleavage resistant control. The peptide was determined using confocal microscopy to be either in subcellular punctae, on the surface of the cells, or in the adjacent extracellular matrix as a light cloud surrounding the 3-D cluster as better visualized by confocal slice of ACPP treatment (Fig. 2F).

ACPPs have more tractable pharmacokinetics than CPPs

To evaluate biodistribution, 10 nmol of either CPP or full length ACPP was injected into the tail vein of mice bearing HT-1080 tumors. Much of the fluorescence of the CPP was immediately retained in the vein near the site of injection and slowly washed out over the following 6 h (Fig. 3A). Fluorescence intensity in the blood decreased to near baseline within minutes after injection (Fig. 3B). Most tissues of mice injected with the CPP appeared dimly fluorescent 30 min after injection and continued to gradually lose fluorescence over the next few hours, suggesting immediate distribution from blood to tissues followed by gradual clearance (Fig. 3C).

In contrast, the ACPP did not remain at the site of injection but rather diffused evenly throughout the tail and tissues (Fig. 3A). The circulation time was much greater for the ACPP, whose blood levels took 30 min to decline to levels reached by the CPP after 3 min (Fig. 3B). Finally, after 30 min the ACPP appeared more fully distributed throughout tissues suggesting that inhibition of the sticky polyarginine by the polyglutamate enabled much greater initial distribution throughout the mouse (Fig. 3C). After 6 h, circulating ACPP peptide was largely washed out of the animals. In ACPP injected animals, greater fluorescence remained, which revealed tumor contrast. These observations suggest that the CPP had limited initial tissue distribution due to its adhesive nature, whereas the ACPPs were able to more fully distribute into tissues allowing an opportunity for enzyme cleavage to unmask the CPP and enable greater retention in target tissues.

In order to quantify the amount of uptake into different critical organs (tumor, muscle, liver, and kidney), we determined the standardized uptake value (SUV) (molality in tissue/molality injected into the animal). Tissue preparation and SUV computation are described in detail in the Experimental section. The measured SUVs for this series of HT-1080-bearing nude mice are shown in Fig. 3D, which reveals a time dependent change and differential distribution between the cleavable ACPP and CPP. The tumor SUV was slightly but not significantly greater for ACPP than CPP at 30 min. Uncleaved and presumably some cleaved peptide washed out by 6 h, resulting in lower SUVs for both peptides. The similarity of CPP and ACPP SUVs measured in tumor homogenates was surprising given that the ACPP consistently gave much higher fluorescence intensity in intact tumors. Possible reasons for this discrepancy are considered in the Discussion. Tumor uptake of ACPP at 6 h was roughly 4-fold greater than in muscle, the most significant adjacent tissue to tumor. Based on the measured SUV, 174 nmol kg^{-1} or 1.7% ID g^{-1} was delivered to tumor from the 10 nmol injection. The liver retained the majority of CPP, presumably because CPP stuck to the liver during the first pass. In contrast the kidney retained the ACPP, presumably due to its inability to adhere to cells until cleaved, resulting in wider body distribution and later renal filtration.

To more clearly understand the pharmacokinetics, the % injected dose can be calculated from the measured SUVs in the liver and kidney, which revealed a significant difference between the CPP and ACPP distribution 30 min after injection and at 6 h. The average weight of the livers from these animals was 1190 mg and for the two kidneys was 333 mg. The measured SUVs using these tissue weights translated into a ten-fold difference (90% *vs.* 8%) in CPP uptake after 30 min in liver and kidney respectively. After 6 h, the uptake in these organs had changed minimally (84% *vs.* 9%). Adding the inhibitory Suc-e_8 decreased liver uptake by a factor of 4.5 and increased kidney uptake by more than a factor of 3 at the early time point (21% *vs.* 28%), this difference was augmented at 6 h (33% *vs.* 48%). Based on these data it became clear that nearly all of the sticky CPP accumulated rapidly in the liver, whereas much of the ACPP remained in circulation after 30 min where it was cleared mainly through the kidney and less by the liver, as evidenced by different SUVs at 6 h. Overall, these results reveal greater ability of ACPPs to reach most target tissues, where cleavage by disease-associated proteases can trigger accumulation, as shown in the accompanying paper (Olson *et al.*)[10b] by directly comparing L-amino acid with cleavage resistant D-amino peptides.

Confocal microscopy of living tissues reveals punctate subcellular distribution of CPPs and ACPPs

CPPs have been advocated for many years as potential vehicles for intracellular delivery beyond endosomes of

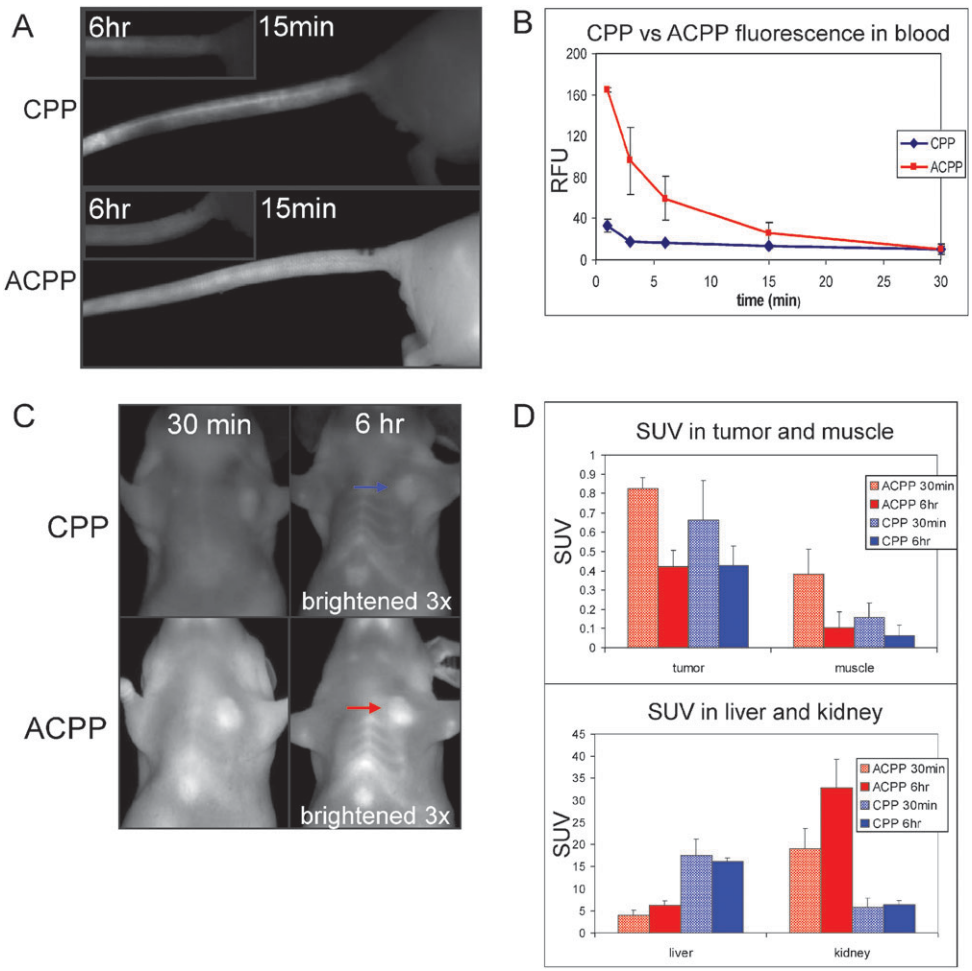

Fig. 3 Comparison of pharmacokinetic tissue distribution between CPP and ACPP following intravenous injection into HT-1080 tumor bearing nude mice reveals differences in peptide distribution. (A) Images showing tail veins of animals injected with CPP (top) and ACPP (bottom) at the indicated time points following injection. (B) Cy5 fluorescence in the blood throughout the first 30 min after injection as an average of three mice for CPP and ACPP. (C) Representative HT-1080 mice injected with CPP and ACPP were imaged at 30 min and 6 h (6 h images brightened 3×). Tumors are indicated by arrows. (D) Standardized uptake value (SUV, molality in tissue/molality injected into the animal) of peptide in tumor, muscle, liver, and kidney, showing changes over time between ACPP and CPP injection. ($n = 4$ for all 6 h mice, $n = 5$ for all organs of 30 min mice, $n = 4$ and $n = 3$ for ACPP and CPP tumors of 30 min mice).

bioactive macromolecules in animals. However, most attempts to demonstrate vehicle delivery have been done in tissue culture, and validation in animals is rarely attempted.[1,2,16] Since most bioactive cargoes would have to reach the cytosol or nucleus to be effective, we used confocal imaging to examine the subcellular distribution of fluorescence signal after IV injection of CPP and ACPP in HT-1080 xenografted mice. Animals that were pre-injected with the ACPP and CPP were reinjected with intravenous Hoechst 33342 (to stain nuclei) and 5 MDa rhodamine dextran (to stain the blood pool) five minutes before sacrifice. At 30 min and 6 h post peptide injection, tissues were removed, kept on ice in HBSS, and imaged using confocal microscopy. Tissues were imaged in the order of kidney, liver, tumor (when applicable) and muscle, mostly due to differing tolerances of live tissue to the effects of hypoxia. Fig. 4 shows confocal slices of the CPP and ACPP in muscle, liver, and kidney. Uptake in the muscle was notably low for both peptides with most of the peptide found in intracellular non-nuclear puncta that were in close proximity to blood vessels. Consistent with gross imaging and SUVs, the liver showed much higher fluorescence for CPP *versus* ACPP at both 30 min and 6 h, though the localization was very similar. Confocal imaging revealed that neither peptide was significantly detectable in the nucleus. Instead, peptide was localized to subcellular puncta and possibly along the sinusoids adjacent to the vascular flow, although this was less clear. Excretion *via* the bile into the duodenum was detected as early as 30 min post injection as shown in ESI, Fig. S2.†

The kidney had the reverse distribution to the liver, with the ACPP accumulating to a much higher degree than the CPP (Fig. 4C), consistent with SUV measurements (Fig. 3D). It was surprising that ACPPs in kidney appeared brighter at 30 min compared to 6 h when the SUV suggested otherwise, an observation that held true for the CPP in the liver. We hypothesize that this difference (microscopy *vs.* homogenate) occurred because when high concentrations of peptide are present, self-quenching of the fluorescent tag is more likely

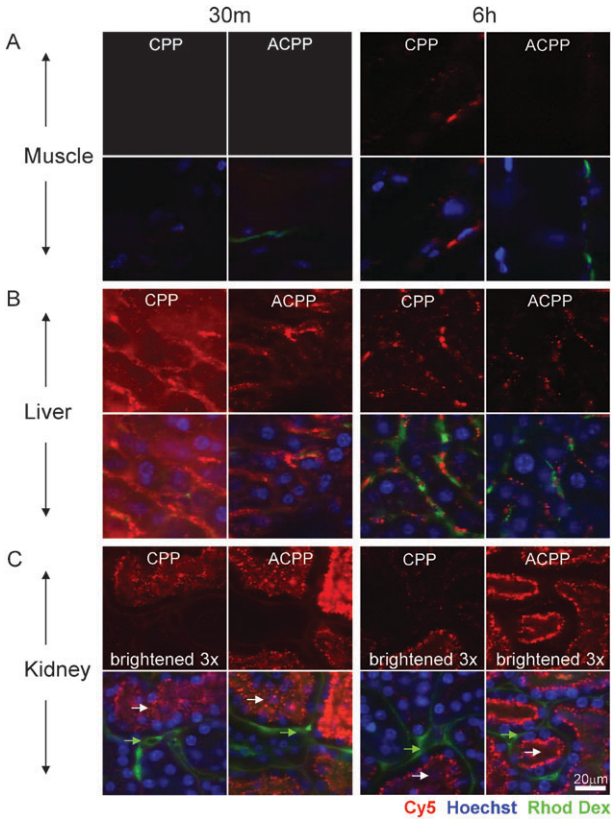

Fig. 4 Confocal microscopy of CPP and ACPP in organs revealed peptide localization to endosomes in nude mice. The figure shows confocal slices of Cy5 peptide (red) and then overlay with nuclei (Hoechst 33342 – blue) and blood pool (rhodamine dextran – green). Images are of muscle (A), liver (B), and kidney (C) at 30 min and 6 h after IV injection of 10 nmol of peptide as specified. No significant nuclear uptake was observed in any tissue for either the CPP or the ACPP. Peptide signal was scaled equally for each organ to visualize subcellular distribution and a difference in scaling in a particular tissue is labeled accordingly. White arrows point to lumen of renal tubules and green arrows point to basal lateral/blood flow region of renal tubules. Scale bar is 20 μm.

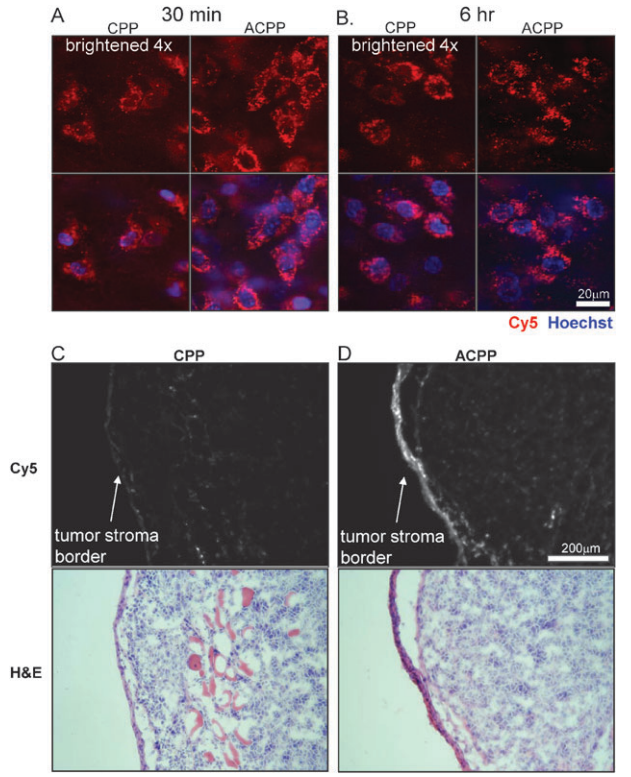

Fig. 5 Confocal microscopy reveals no significant nuclear uptake of ACPP or CPP in HT-1080 xenografts. Confocal slice of HT-1080 tumors from mice injected with CPP and ACPP at 30 min (A) and 6 h (B). Mice were injected with Cy5 peptide (red) at 30 min or 6 h before imaging and Hoechst 33342 nuclear stain (blue) 5 min before imaging to demonstrate that ACPP uptake is in cytoplasmic perinuclear structures but not in nuclei. Upper image is Cy5 peptide alone and lower image shows overlay with Hoechst. The CPP images were scaled brighter by a factor of 4 to visualize intracellular peptide containing punctae. Scale bar is 20 μm. (C, D) Show Cy5 fluorescence of frozen sections from mice 6 h after injection of CPP or ACPP, highlighting greater uptake with ACPP particularly at leading stromal edge of tumors. Scale bar 200 μM.

to occur, thus affecting quantitative imaging. Self-quenching was observed in SUV homogenates at very high concentrations but was accounted for using SUV standard curves. Renal excretion of the ACPP was evidenced by the fluorescence signal of the urine present in the bladder 30 min after injection (ESI, Fig. S2†) but this was not quantified. The kidney uptake was predominantly in luminal puncta (white arrows) of the tubules, suggesting that the 2–5 kDa peptides were filtered and endocytosed in the renal tubules and completely excreted. Again there was no detectable peptide in the nuclei of kidney cells for either peptide (Fig. 4C). For each tissue a short time series was taken to confirm that the fluorescence contained in intracellular vesicles continued to move around inside the cells, suggesting that the cells were alive (data not shown). When the tissues sat on coverslips as dry mounts over time, the peptide shifted its distribution to the nuclei as shown in the kidney (ESI, Fig. S3†), likely due to loss of membrane integrity and/or cell death. These observations highlight the ease with which misassignment of peptide localization occurs unless properly controlled for.

Confocal microscopy reveals no obvious detectable nuclear uptake of ACPPs and CPPs in live tumor and stroma of xenografted mice

By thorough visual inspection of confocal stacks of various tissues including tumors, it became evident that neither ACPP nor CPP yielded detectable nuclear uptake in intact living cells, as discussed above (Fig. 4). Fluorescence signal was about four times higher for the ACPP than for the CPP (Fig. 5A and B), but was mostly in perinuclear puncta for both peptides. Nuclear uptake was below the detection limit as confirmed by scrolling through z sections of confocal stacks (Fig. 5A and B). Many nuclei, especially in the core of the tumor, failed to label with Hoechst 33342. Perhaps this small molecule is eliminated from the circulation before it reaches the poorly perfused interior of a xenograft. However, the cells at the tumor stroma/capsule boundary that had the highest level of peptide uptake had detectable Hoechst labeled nuclei. Because endosomal escape and nuclear uptake of CPPs in monolayer tissue culture often require concentrations of

Table 1 Summary of CPP and ACPP acute toxicity in mice. Nude mice were IV injected with peptide and observed for acute toxicity resulting in rapid death. Mouse survival of immediate period after injection was recorded, each showing no signs of moribundity or significant weight loss for at least 2 days post injection. Unlabeled peptide injected, dose injected IV, range of mice mass, time of death, and number survived (minimal 24 h with no signs of toxicity) are listed in the Table

Peptide	Dose	Mouse mass (range)	Time of death	Survived
r_9 CPP	2.5 μmol kg^{-1} (53–65 nmol)	21.7–26.0 g	15–20 min, $n = 1$	4/5
	5 μmol kg^{-1} (105–117 nmol)	21.0–25.7 g	<3 min, $n = 5$	0/5
PLGLAG cleavable ACPP	10 μmol kg^{-1} (220–266 nmol)	22.3–26.6 g	NA	5/5
	20 μmol kg^{-1} (352–480 nmol)	16.0–24.0 g	10–20 min, $n = 5$	0/5
$(PEG2)_2$ uncleavable ACPP	10 μmol kg^{-1} (182, 202 nmol)	20.6–23.3 g	NA	2/2
	20 μmol kg^{-1} (405 nmol)	20.2–21.2 g	NA	2/2
	50 μmol kg^{-1} (1100–1280 nmol)	22.0–25.6 g	NA	3/3

several μM or more,[16,17] we injected one mouse with 100 nmol or 5 μmol kg^{-1} of ACPP, 10 times the usual dose, but there was still no detectable nuclear uptake in any tissue (data not shown). Presumably the local concentration of free CPP stayed well below the threshold of several μM necessary for cytosol and nuclear uptake in culture, because of a lack of complete ACPP proteolysis and an excess of binding sites within compacted tissue *in vivo*. However the final concentration determined for CPP in the liver and ACPP in the kidney was up to 8–17 μmol kg^{-1} based on SUV assuming 20–25 g mouse from just a 10 nmol injection (Fig. 3D). Further consideration of direct systemic injection of free CPPs at $\geq$ 5 μmol kg^{-1} (100 nmol) was impractical due to systemic toxicity (see below). The tumor stroma/capsule as shown in Fig. 5A and B was much brighter for the ACPP than for the CPP, as more clearly shown by fluorescence and hematoxylin/eosin histology (Fig. 5C and D). This difference reflects protease dependent activation and uptake as analyzed further in the accompanying paper (Olson *et al.*).[10b]

ACPPs decrease acute toxicity of CPPs because of the linked polyanionic inhibitory domain

Although CPPs have been proposed for many years as vehicles for macromolecular drug delivery very little has been reported regarding their systemic toxicity. Because large quantities of peptides were required for such studies and to avoid toxicity from the fluorescent tag, three unlabeled peptides were synthesized with C-terminal amides: r_9 (CPP), Suc-e_8-*x*PLGLAG-r_9 (cleavable ACPP), and Suc-e_8-$(PEG2)_2$-r_9 (uncleavable control, where PEG2 = $–NH(CH_2CH_2O)_2CH_2CO–$). Acute toxicities are summarized in Table 1. At an intravenous dose of 100 nmol or 5 μmol kg^{-1}, 10-fold higher than the imaging dose of 10 nmol, the CPP was acutely toxic. These animals appeared to go into shock with visibly dilated blood vessels and died of respiratory collapse within one minute after bolus injection. The anesthesia was then changed from injectable ketamine/midazolam to isoflurane, a volatile anesthetic that is more rapidly reversible (30 s to 1 min). Under these conditions and with reduction of the CPP dose to 2.5 μmol kg^{-1}, four out of five mice survived the injection. Clinically, however, they showed signs of respiratory distress, which was resolved as they recovered from anesthesia after about one minute. Subsequently the animals showed signs of visible vasodilation and were slightly sedated but responsive to stimulation for 10–20 min after injection. After this initial recovery period, the mice appeared perfectly normal and lost no significant weight over the following 24 h period. When the injection was increased to 5 μmol kg^{-1}, under the same anesthesia conditions, none of five mice survived the first few minutes. Death appeared to be due to immediate respiratory failure.

We hypothesized that the systemic toxicity of the CPP was associated with the large positive charge causing mast cell degranulation as previously discussed.[18] We tested our hypothesis that the polyanionic motif of ACPP would inhibit this acute toxicity by injecting a starting dose of 5 μmol kg^{-1}. Indeed, this dose appeared to have no acute effect. When the dose was increased to 10 μmol kg^{-1} all five mice survived but troubling clinical signs began to appear, including vasodilation and sedation beginning two to three minutes after recovery from anesthesia. Animals slowly became unresponsive to toe pinch and remained in a sedated state for 30 min to 90 min, after which they recovered full alertness and behaved normally. The mice lost no more than 1 g of weight over the first 24 h and the surviving mice continued to thrive. The dose was then increased to 20 μmol kg^{-1} and none of five mice survived longer than 15 min at this increased dose. Death appeared to be due to respiratory failure following cardiovascular collapse, as described earlier for CPPs but was delayed for ACPPs.

Although the maximum tolerated dose of the cleavable ACPP was about 4-fold higher than that of the CPP, the symptoms of toxicity were roughly similar though delayed, suggesting that the toxicity of the cleavable ACPP may be due to a fraction of molecules undergoing nonspecific proteolysis and release of their CPP components. If so, the control uncleavable peptide should have even less systemic toxicity. To test this hypothesis, two mice were initially injected with 10 μmol kg^{-1} of the uncleavable control and both survived. The mice woke up within the first minute with normal behavior and no signs of vasodilation. At 20 μmol kg^{-1} 2/2 survived with no clinical signs of stress. Mice were then injected with 50 μmol kg^{-1} and there was no sign of toxicity in 3/3 mice. This dose is 20-fold greater than the maximum tolerated dose of the CPP and indicates that the tandemly fused anionic segment reduces CPP toxicity by at least this amount. We did not increase the dose beyond 50 μmol kg^{-1} of the uncleavable control because of the large quantities of peptide required (over 1 μmol per animal) and because an uncleavable control has no diagnostic or therapeutic relevance *per se*, but serves mainly to suggest how low the systemic toxicity might ultimately be if the linker were selectively cleaved only within the tumor.

After obtaining these unexpected experimental results, the question still remained whether this toxicity of CPP and cleavable ACPP was due to rapid bolus which could be attenuated by intraperitoneal (IP) administration. Two animals were injected with 20 μmol kg^{-1} of CPP. Initially they became slightly flushed and unresponsive for 5–10 min then at about 15 min both died as described for the IV ACPP at 10 μmol kg^{-1}. For the cleavable ACPP, a mouse injected with a 20 μmol kg^{-1} dose died after slow onset of clinical signs, but onset took more than an hour. Therefore IP administration does delay and attenuate the toxicity of both CPP and ACPP, likely due to slowed systemic delivery, but did not eliminate toxicity.

Discussion

Activatable cell-penetrating peptides represent a novel strategy for targeting imaging contrast agents and therapeutic agents for cancer. This approach requires that uptake of CPPs be inhibitable by covalent linkage of a complementary polyanionic peptide, and that such inhibition is reversible by cleavage of the linker, *e.g.* by proteases. Our initial publication[10a] demonstrated the basic feasibility of ACPPs but left many questions unanswered, some of which we address here.

The idea that the polyanion blocks the polycation only as long as they are covalently tied to each other is qualitatively plausible but needs quantitative justification. Determination of the K_d for r_9–e_9 binding confirms that this value (~6 μM) lies safely between the effective molarity (~50 mM) enforced by our typical linker with 25 rotatable bonds and the probable free concentrations of each peptide attained *in vivo* (<0.4 μM). But these numbers provide some prospective guidance, not just retrospective justification. They suggest that longer linkers with as many as 50 rotatable bonds should still work, because the effective molarity would still be ~18 mM.[14] Such extra length could be useful, either to allow substrate recognition sequences longer than six amino acids, or to incorporate extra spacers to enable the peptide to adopt a more linear conformation inside the protease active site. However, major increases in the length of the polyarginine and polyglutamate repeats could well make dissociation too inefficient or too slow after linker cleavage. Major shortening of those repeats is also not advisable, because efficiency of polyarginine CPPs falls off steeply below about eight arginines.[19] A naked polynucleotide chain is likely to be quite good at binding to and neutralizing polyarginine of the same number of charges, so polyarginine-mediated delivery of DNA or RNA will probably require shielding of the nucleic acid or provision of excess positive charges.

Tumors are much more brightly stained *in vivo* by ACPPs than equimolar CPPs, both imaged 6 h after IV administration (Fig. 3C and 5B–D; also Fig. 3B of the accompanying paper, Olson *et al.*[10b]). Thus ACPPs are considerably superior to CPPs for epifluorescence imaging, the way optical probes are normally evaluated. However, in this paper we have also introduced SUVs measured by fluorescence after homogenization of bulk tissue in SDS. Such SUVs do not yet show significantly higher tumor uptake for ACPPs over CPPs (Fig. 3D). Some of the discrepancy might be explained by the tendency of the ACPP to preferentially light up the outer edge of the tumor (Fig. 5D), which is the region most visible by macroscopic epifluorescence. Another speculative possibility is that much of the CPP is sufficiently highly concentrated, perhaps on the walls of the vasculature, that the Cy5 fluorescence undergoes self-quenching. Both forms of localization would be destroyed upon tissue homogenization.

Although our previous paper showed cells in 2-D culture with diffuse cytosolic and nuclear uptake of pre-cleaved ACPPs,[10a] subsequent experiments in 3-D cultures and tumors *in vivo* have consistently revealed that practically all the visible fluorescence comes from perinuclear punctae, presumably endosomes. We believe the main difference from earlier studies arose from the sudden exposure of naked cells to an undepletable supply of 1.25 μM CPP, allowing high enough accumulations in the endosomes to disrupt those organelles. In the present study, the CPP is gradually generated by *in situ* cleavage of the ACPP and is buffered by a high density of neighboring cells and extracellular matrix. Therefore endosomal concentrations may never reach the threshold required for membrane disruption though final concentration reached in tissue has been observed beyond 8–17 μmol kg^{-1}. This reasoning suggests that the only way *in vivo* to achieve the levels of CPP currently necessary to disrupt endosomes or be taken by disruption of membrane potential (possibly in an endosome independent way)[13,20] would be by localized administration of high concentrations directly into a particular tissue of interest. Systemic delivery of cargoes directly linked to simple CPPs will not reach the cytoplasm or nucleus because the CPP is diluted over too many binding sites and is already toxic at modest doses. ACPPs are more tissue-specific and less toxic, but enzymatic release of the active CPP is gradual and may not be stoichiometric. Efficient *in vivo* delivery to the cytoplasm and nucleus will probably require cargoes that are either much more potently endosomolytic or that release membrane-permeant fragments. Fortunately, many applications of ACPPs, *e.g.* macroscopic imaging for tumor diagnosis, do not require endosomal escape.

The systemic toxicity of the free polyarginine CPP was somewhat surprising. The detailed mechanism remains to be elucidated, but toxicity is inhibited by attachment of the polyglutamate domain just as cellular uptake is. Therefore future improvements in selectivity that reduce the cleavage of the ACPP in non-tumor organs should not only increase tumor contrast but decrease systemic toxicity. The accompanying paper examines selective cleavage in greater detail.[10b]

Experimental

Peptide synthesis and fluorophore labeling

Peptides for imaging experiments were synthesized on an automatic peptide synthesizer (Perceptive Biosystems Pioneer or PTI Prelude) using standard protocols for fluorenylmethoxycarbonyl (Fmoc) solid-phase synthesis. They were then labeled with Cy5 using Cy5 monomaleimide or Cy5 mono NHS ester (GE Healthcare) and then purified by HPLC. Exact sequences for the CPP, the ACPP and the cleavage resistant D-amino

acid control were r_9-c(Cy5)-NH_2 (r_9Cy5), Suc-e_8-*x*PLGLAG-r_9-c(Cy5)-NH_2, and Suc-e_8-*x*-plglag-r_9-k(Cy5)-NH_2, where D-amino acids are denoted in lower case and *x* denotes 6-aminohexanoyl. The peptides for toxicity experiments, purchased from Anaspec Inc. (San Jose, CA), were r_9-NH_2 (simple r_9 CPP), Suc-e_8-*x*PLGLAG-r_9-NH_2 (MMP cleavable ACPP), and Suc-e_8-$(PEG2)_2$-r_9-NH_2 (uncleavable control). After purification by HPLC, their concentrations were determined by weight and confirmed by amino acid analysis (Alphalyse, Palo Alto, CA). Peptide structures were confirmed by mass spectrometry

Isothermal titration calorimetry (ITC)

All peptide solutions were in 20 mM Tris, pH 7.40, 150 mM NaCl. Peptide concentrations were determined by amino acid analysis. ITC runs were performed on a VP-ITC (Microcal LLC, Northampton, MA) instrument at 37 °C. Suc-e_8-NH_2 (0.230 mM) in the syringe was titrated into r_9-NH_2 (0.013 mM) (these two peptides will be referred to as Suc-e_8 and r_9). A blank run of Suc-e_8 into buffer alone was subtracted from the experimental data to obtain the final binding isotherm. The data were analyzed using Origin software supplied by Microcal. ΔH and K_a values, along with their corresponding standard deviations, were determined directly by nonlinear least squares fit of the titration data, fixing *n* (stoichiometry of the complex) at 1.0. Ten runs were pooled to calculate the mean and standard deviation for the K_d, with a matched control (no peptide spiked into chamber) done the same day. The peptides were reversed with r_9 in the chamber and Suc-e_8 titrated in, yielding similar results.

Enzyme cleavage assay

Recombinant MMP-1, MMP-2, MMP-3, MMP-7, MMP-8, MMP-9, MT1-MMP (MMP-14), cathepsin B, thrombin, plasmin, tissue plasminogen activator (tPA), prostate specific antigen (PSA), and thrombin were obtained from EMD. Urokinase (uPA) was from Sigma and neprilysin from R&D Systems Inc. These enzymes were activated by vendors' recommended protocols if needed, then incubated at 50 nM with 3 μM peptide for 30 min at 37 °C. Cleavage was performed in a 20 mM Tris buffer with 150 mM NaCl and 2 mM $CaCl_2$ at pH 7.4 for all enzymes except for cathepsin B, which was tested in 50 mM sodium acetate at pH 5.0. Samples were diluted into SDS tricine loading buffer, boiled, and run on 10–20% tricine buffered polyacrylamide gels (Invitrogen). Gels were imaged to detect Cy5 labeled peptide and % peptide cleavage was determined from average signal measurements using Image J (NIH) done in triplicate.

3-D tissue culture

HT-1080 fibrosarcoma (ATCC) and MDA-MB-231 human adenocarcinoma (Bissell lab) were cultured as monolayers in Eagle's Minimal Essential Medium with 10% fetal bovine serum at pH 7.2. For 3-D culture, 1000–5000 cells were plated in 2 mg mL^{-1} Matrigel (BD biosciences) on top of a base coat in 96 well plates to keep cells suspended. When clusters reached 75–200 μm diameter, they were treated for 20–24 h with 1.5 μM Cy5 labeled ACPP or control peptides, with or without MMP inhibitor GM6001 (EMD Biosciences), and a 1% final concentration of DMSO. Clusters were then treated with 1 μg mL^{-1} of calcein green AM (Invitrogen) and 10 μg mL^{-1} propidium iodide (EMD) to label live and dead cells, respectively and subsequently washed three times. Cell clusters were imaged at low power on a fluorescence dissecting microscope (Lumar, Zeiss) for quantification of multiple clusters, or imaged by laser scanning confocal microscopy for higher resolution (LSM5 Live, Zeiss). Average Cy5 intensity per cluster was measured from 20–40 clusters distributed over three images taken from duplicate treatments. Confocal images are presented as maximum projections of 50 images acquired at 1 μm depth intervals.

Mouse models

Pharmacokinetic distribution studies of ACPP and CPPs were performed in athymic nude mice (Charles River Labs) containing xenografts of HT-1080 tumors prepared by injection of two million cells (ATCC) into the left mammary fat pad 5–7 days before peptide injection. For toxicity studies, naïve athymic nude mice were used. All procedures were approved by the UCSD Institutional Animal Care and Use Committee.

Whole animal imaging

After tail vein injection, mice were imaged at different time points using a small animal imager (Maestro, Cambridge Research Instruments). Images were acquired with 640 ± 20 nm excitation and the emission filter tuned to 700 nm (bandwidth 40 nm), augmented by a 700 nm long pass filter, with exposure times between 300 ms and 1 s. Blood was collected at various time points from the tail artery into capillary tubes, which were imaged for Cy5 fluorescence on the Maestro. For live animal imaging, the mice were anesthetized with 125 mg kg^{-1} of ketamine and 62.5 mg kg^{-1} of midazolam.

Standardized uptake values

After euthanasia, organs were harvested, cut into 30 mg pieces, homogenized in 100 μL 10 mM Tris buffer (pH 7.6) with 1% SDS, boiled for 10 min, centrifuged at 20 500× *g* for 10 min and frozen. Tissues were then imaged while frozen on the Maestro. Integrated intensities of tissues were collected using Image J software and relative values were adjusted using a fluorescence calibration standard (USFS-336 Orange Fluorescence, Labsphere Inc.). Peptide concentration was determined from tissue fluorescence using a tissue specific standard curve (HT-1080 tumor, liver, kidney and muscle from nude mice) with known amounts of r_9Cy5 peptide spiked into tissue samples and processed as above. The 3 parameter exponential rise to max ($f = y + a^*(1 - \exp(-b^*x))$; Sigmaplot) equation was used for standard curves due to nonlinearity of fluorescence at high concentrations >1 μmol kg^{-1}. From these data the SUV was calculated as (moles/g tissue)/(moles injected/weight of animal).

Confocal imaging of live mouse tissues

Animals were injected intravenously with 250 μg of Hoechst 33342 (Invitrogen) and 800 μg of 2 MDa rhodamine dextran

(Invitrogen) 5 min before sacrifice. Organs were then removed and kept on ice in HBSS until image. Organs were then placed on a coverslip and imaged by confocal microscopy (LSM 5 Live, Zeiss). Tissues were imaged in the order of kidney, liver, tumor, and muscle within 30 min of sacrifice to minimize tissue death. Images were acquired as 3-D stacks with 5–60 μm penetration into tissue. Cy5, Hoechst, and rhodamine were excited with 630 nm, 405 nm, and 535 nm lasers while emission was acquired with 650 nm LP, 420 nm LP, and 550 nm LP filters, respectively.

Toxicity of CPP and ACPPs in mice

Peptides dissolved in 50 μL of water were injected into the tail vein under isoflurane anesthesia. For IP injection of peptide mice were not anesthetized. Immediately after injection, isoflurane was removed and mice were allowed to wake up under observation. Body masses were measured before and 24 h after injection (if the animal survived injection) to detect significant weight loss due to toxicity. Toxicity was assayed both qualitatively and quantitatively by clinical observation of healthy *vs*. moribund behavior, and death.

Abbreviations

CPP	cell penetrating peptide
ACPP	activatable cell penetrating peptide
MMP	matrix metalloproteinase
SUV	standardized uptake value

Acknowledgements

We thank Mina Bissell for instruction on 3-D cultures and cells; Perla Acaira for processing of SUV tissues; Mike Whitney for assistance in peptide synthesis and discussion; Jessica Crisp for expertise and assistance performing enzyme cleavage assay and important discussion; Qing Xing for assistance in peptide synthesis. This work was supported by grant W81XWH-05-1-0183 from the Department of Defense Breast Cancer Research Program.

References

1 V. P. Torchilin, Tat peptide-mediated intracellular delivery of pharmaceutical nanocarriers, *Adv. Drug Delivery Rev*., 2008, **60**, 548–558.
2 L. N. Patel, J. L. Zaro and W. C. Shen, Cell penetrating peptides: intracellular pathways and pharmaceutical perspectives, *Pharm. Res*., 2007, **24**, 1977–1992.
3 M. Lundberg and M. Johansson, Is VP22 nuclear homing an artifact?, *Nat. Biotechnol*., 2001, **19**, 713–714.
4 J. P. Richard, K. Melikov, E. Vives, C. Ramos, B. Verbeure, M. J. Gait, L. V. Chernomordik and B. Lebleu, Cell-penetrating peptides. A reevaluation of the mechanism of cellular uptake, *J. Biol. Chem*., 2003, **278**, 585–590.
5 S. R. Schwarze, A. Ho, A. Vocero-Akbani and S. F. Dowdy, *In vivo* protein transduction: delivery of a biologically active protein into the mouse, *Science*, 1999, **285**, 1569–1572.
6 E. L. Snyder, B. R. Meade and S. F. Dowdy, Anti-cancer protein transduction strategies: reconstitution of p27 tumor suppressor function, *J. Controlled Release*, 2003, **91**, 45–51.
7 J. C. Mai, Z. Mi, S. H. Kim, B. Ng and P. D. Robbins, A proapoptotic peptide for the treatment of solid tumors, *Cancer Res*., 2001, **61**, 7709–7712.
8 E. L. Snyder, B. R. Meade, C. C. Saenz and S. F. Dowdy, Treatment of terminal peritoneal carcinomatosis by a transducible p53-activating peptide, *PLoS Biol*., 2004, **2**, E36.
9 E. A. Dubikovskaya, S. H. Thorne, T. H. Pillow, C. H. Contag and P. A. Wender, Overcoming multidrug resistance of small-molecule therapeutics through conjugation with releasable octaarginine transporters, *Proc. Natl. Acad. Sci. U. S. A*., 2008, **105**, 12128–12133.
10 (*a*) T. Jiang, E. S. Olson, Q. T. Nguyen, M. Roy, P. A. Jennings and R. Y. Tsien, Tumor imaging by means of proteolytic activation of cell-penetrating peptides, *Proc. Natl. Acad. Sci. U. S. A*., 2004, **101**, 17867–17872; (*b*) E. S. Olson, T. A. Aguilera, T. Jiang, L. G. Ellies, Q. T. Nguyen, E. Wong, L. Gross and R. Y. Tsien, *In vivo* characterization of activatable cell penetrating peptides for targeting protease activity in cancer, *Integr. Biol*., 2009, DOI: 10.1039/b904890a.
11 V. Polyakov, V. Sharma, J. L. Dahlheimer, C. M. Pica, G. D. Luker and D. Piwnica-Worms, Novel Tat-peptide chelates for direct transduction of technetium-99m and rhenium into human cells for imaging and radiotherapy, *Bioconjugate Chem*., 2000, **11**, 762–771.
12 H. J. Lee and W. M. Pardridge, Pharmacokinetics and delivery of tat and tat–protein conjugates to tissues *in vivo*, *Bioconjugate Chem*., 2001, **12**, 995–999.
13 M. Kosuge, T. Takeuchi, I. Nakase, A. T. Jones and S. Futaki, Cellular internalization and distribution of arginine-rich peptides as a function of extracellular peptide concentration, serum, and plasma membrane associated proteoglycans, *Bioconjugate Chem*., 2008, **19**, 656–664.
14 C. Galli and L. Mandolini, The role of ring strain on the ease of ring closure of bifunctional chain molecules, *Eur. J. Org. Chem*., 2000, 3117–3125.
15 G. Kasper, M. Reule, M. Tschirschmann, N. Dankert, K. Stout-Weider, R. Lauster, E. Schrock, D. Mennerich, G. N. Duda and K. E. Lehmann, Stromelysin-3 over-expression enhances tumourigenesis in MCF-7 and MDA-MB-231 breast cancer cell lines: involvement of the IGF-1 signalling pathway, *BMC Cancer*, 2007, **7**, 12.
16 E. Vives, Present and future of cell-penetrating peptide mediated delivery systems: "is the Trojan horse too wild to go only to Troy?", *J. Controlled Release*, 2005, **109**, 77–85.
17 J. S. Wadia and S. F. Dowdy, Transmembrane delivery of protein and peptide drugs byTAT-mediated transduction in the treatment of cancer, *Adv. Drug Delivery Rev*., 2005, **57**, 579–596.
18 C. F. Albright, N. Graciani, W. Han, E. Yue, R. Stein, Z. Lai, M. Diamond, R. Dowling, L. Grimminger, S. Y. Zhang, D. Behrens, A. Musselman, R. Bruckner, M. Zhang, X. Jiang, D. Hu, A. Higley, S. Dimeo, M. Rafalski, S. Mandlekar, B. Car, S. Yeleswaram, A. Stern, R. A. Copeland, A. Combs, S. P. Seitz, G. L. Trainor, R. Taub, P. Huang and A. Oliff, Matrix metalloproteinase-activated doxorubicin prodrugs inhibit HT1080 xenograft growth better than doxorubicin with less toxicity, *Mol. Cancer Ther*., 2005, **4**, 751–760.
19 P. A. Wender, D. J. Mitchell, K. Pattabiraman, E. T. Pelkey, L. Steinman and J. B. Rothbard, The design, synthesis, and evaluation of molecules that enable or enhance cellular uptake: peptoid molecular transporters, *Proc. Natl. Acad. Sci. U. S. A*., 2000, **97**, 13003–13008.
20 J. B. Rothbard, T. C. Jessop, R. S. Lewis, B. A. Murray and P. A. Wender, Role of membrane potential and hydrogen bonding in the mechanism of translocation of guanidinium-rich peptides into cells, *J. Am. Chem. Soc*., 2004, **126**, 9506–9507.